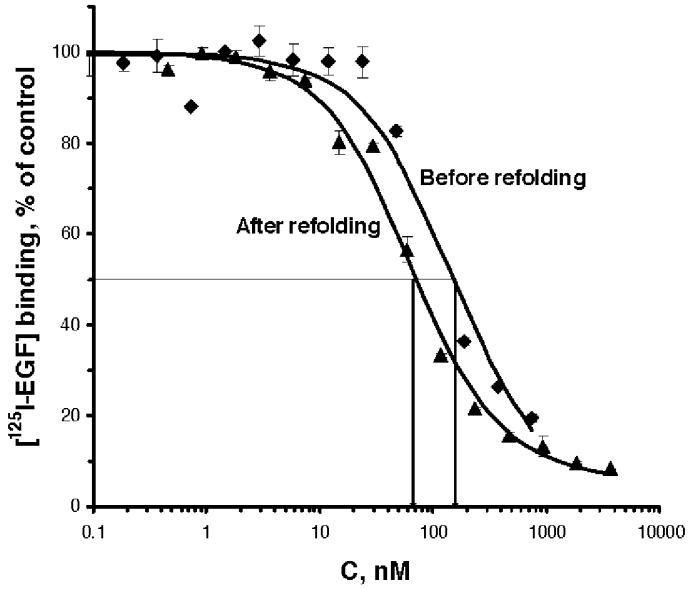
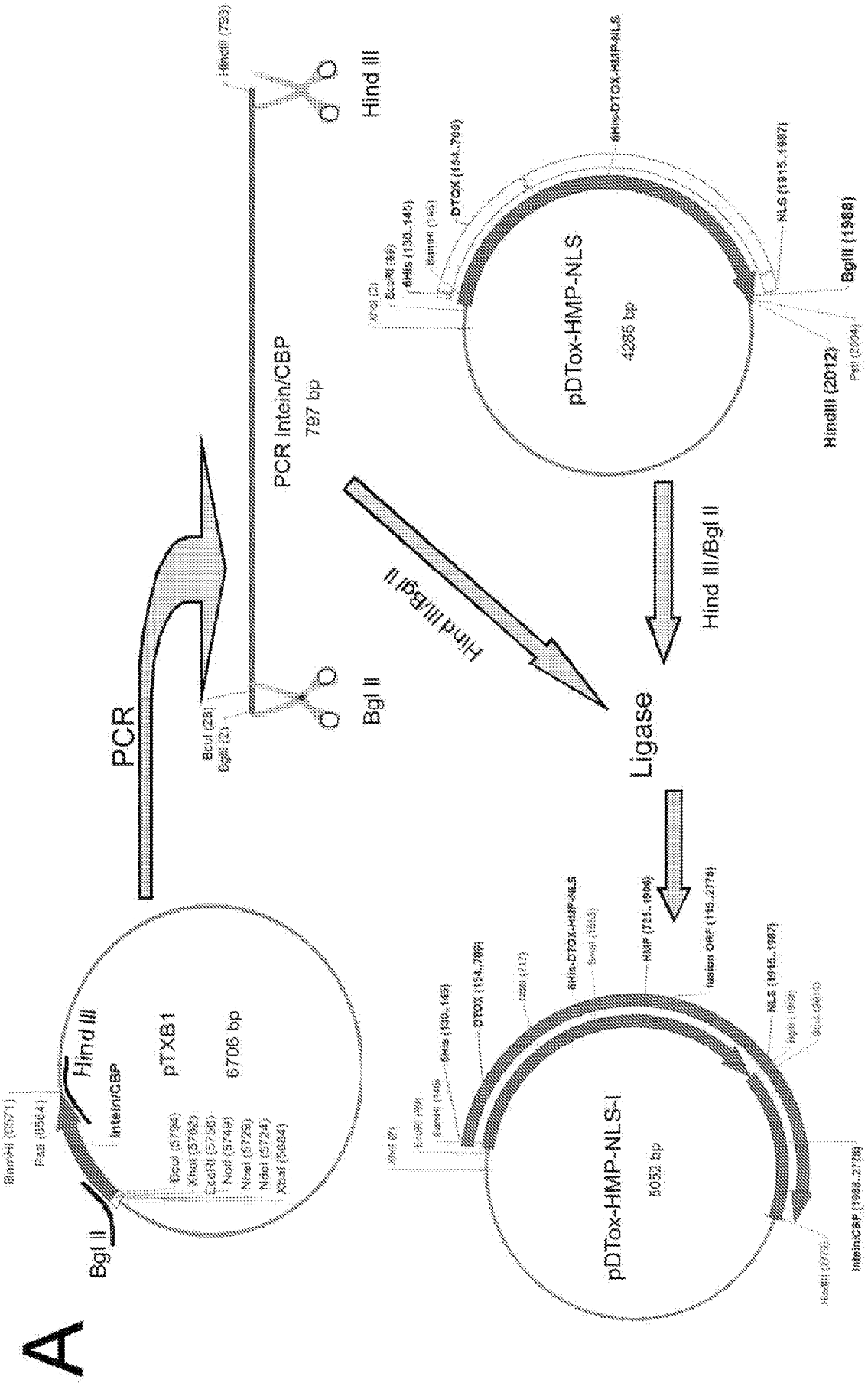


Fig. 1. Effect of MTP posttranslational treatment on affinity of its ligand module to cell receptor. Displacement of [^{125}I]iodo-EGF (2 nM) by DTox-HMP-NLS-EGF before (◆) and after (▲) refolding from EGFR receptors of A431 human epidermoid carcinoma cells. [^{125}I]iodo-EGF bound to A431 cell surface receptors with affinity constant of 0.15±0.02 nM^{-1}. Affinity constants for MTP binding with receptor were 0.019±0.003 nM^{-1} before refolding and 0.054±0.005 nM^{-1} after refolding.


A
pTXB1
6706 bp
Hind III
Bgl II
intein/CBP
PCR
PCR intein/CBP
797 bp
Hind III
Bgl II
Hind III/Bgl II
Ligase
pDTox-HMP-NLS
4265 bp
pDTox-HMP-NLS-I
5052 bp

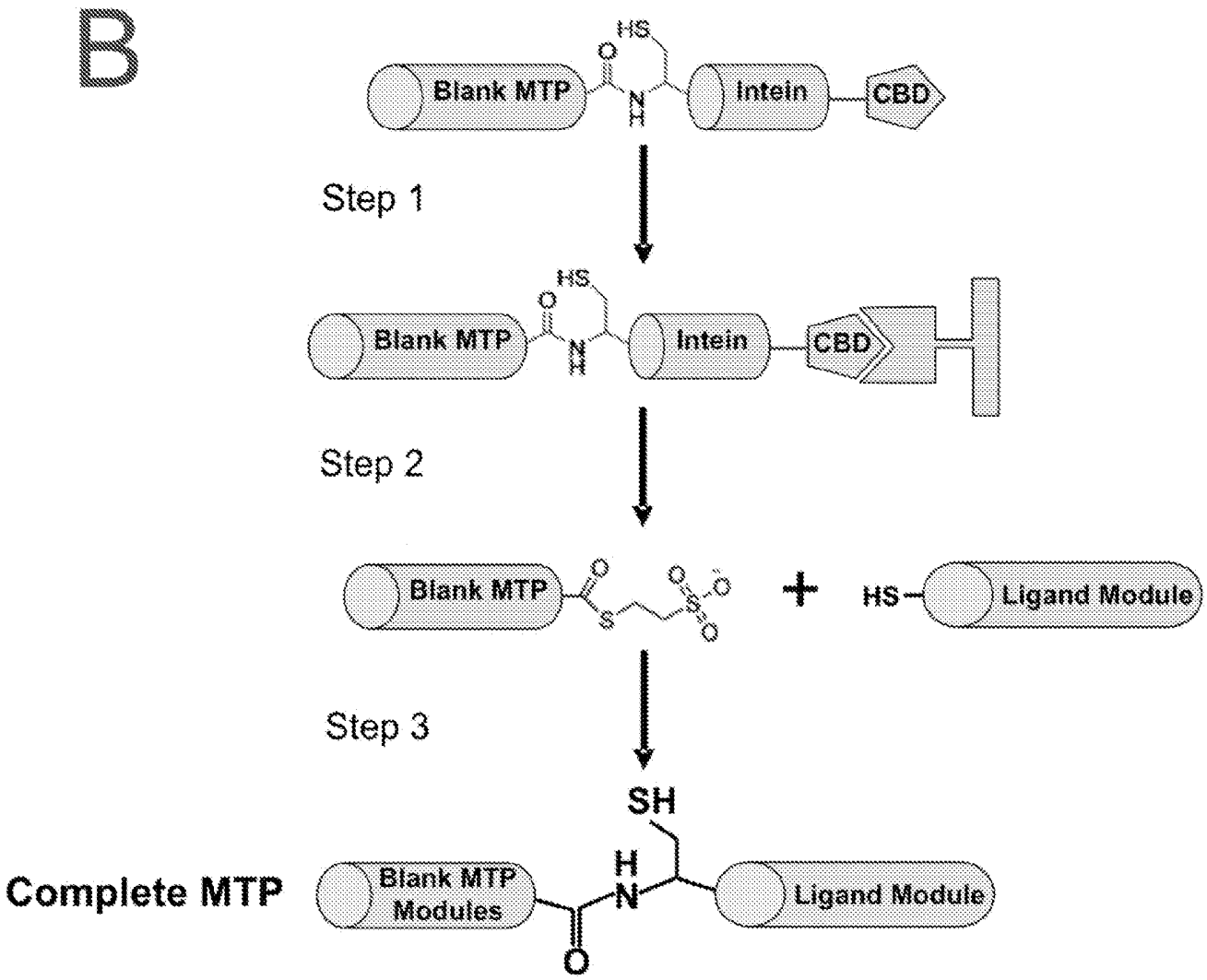


Fig. 2. Schematic representation of construction of an MPT encoding plasmid possessing intein and CBD (chitin-binding domain)-encoding regions, purification of the "blank" MTP, and the liganding step of the non-liganded MTP to the polypeptide ligand.

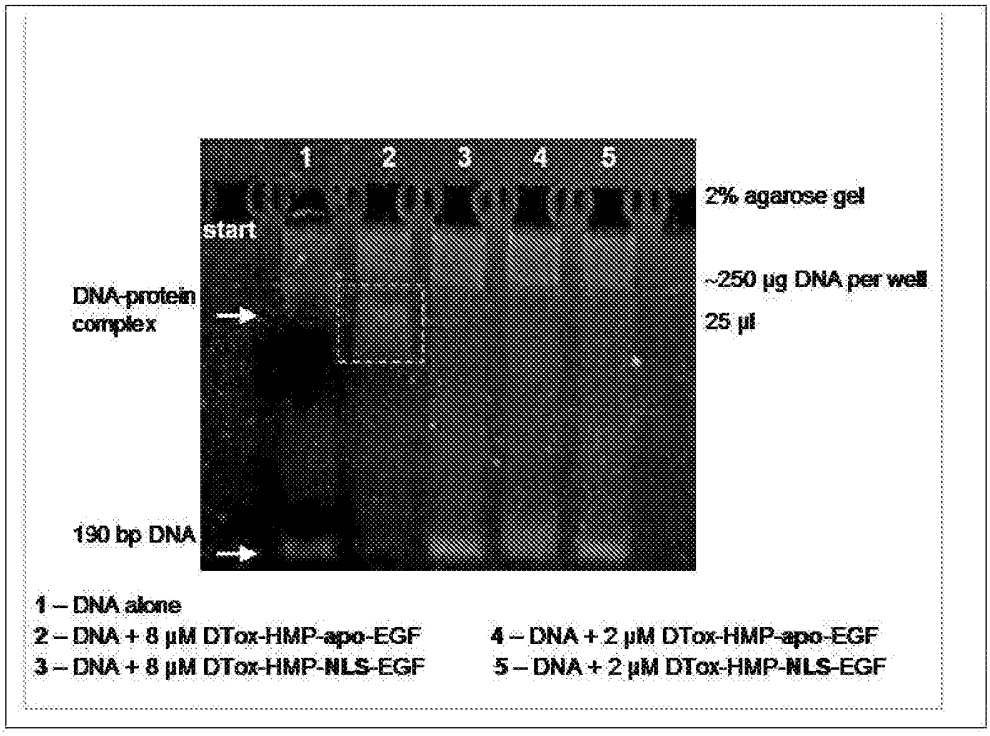


Fig. 3. Gel-shift assay with MTP containing apoptin fragment, DTox-HMP-apo-EGF, and lacking it, DTox-HMP-NLS-EGF.

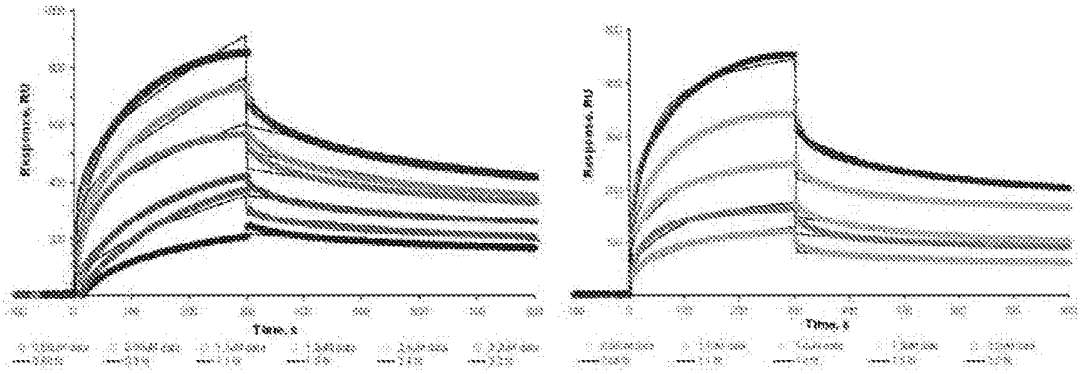


Fig. 4. the interaction of DTox-HMP-apo-EGF (left graph) and DTox-HMP-NLS-EGF (right graph) with plasmid DNA assayed using surface plasmon resonance method on SA chip. Affinity constants for MTP binding with DNA were 0.26±0.06 μM^{-1} for DTox-HMP-apo-EGF and 0.011±0.002 μM^{-1} for DTox-HMP-NLS-EGF.

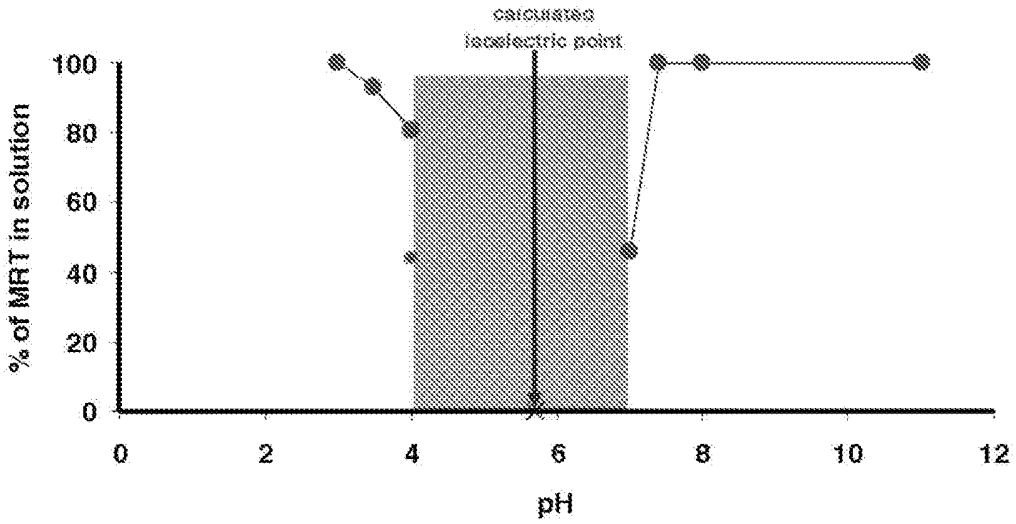


Fig. 5. Solubility of MTP at different pH conditions

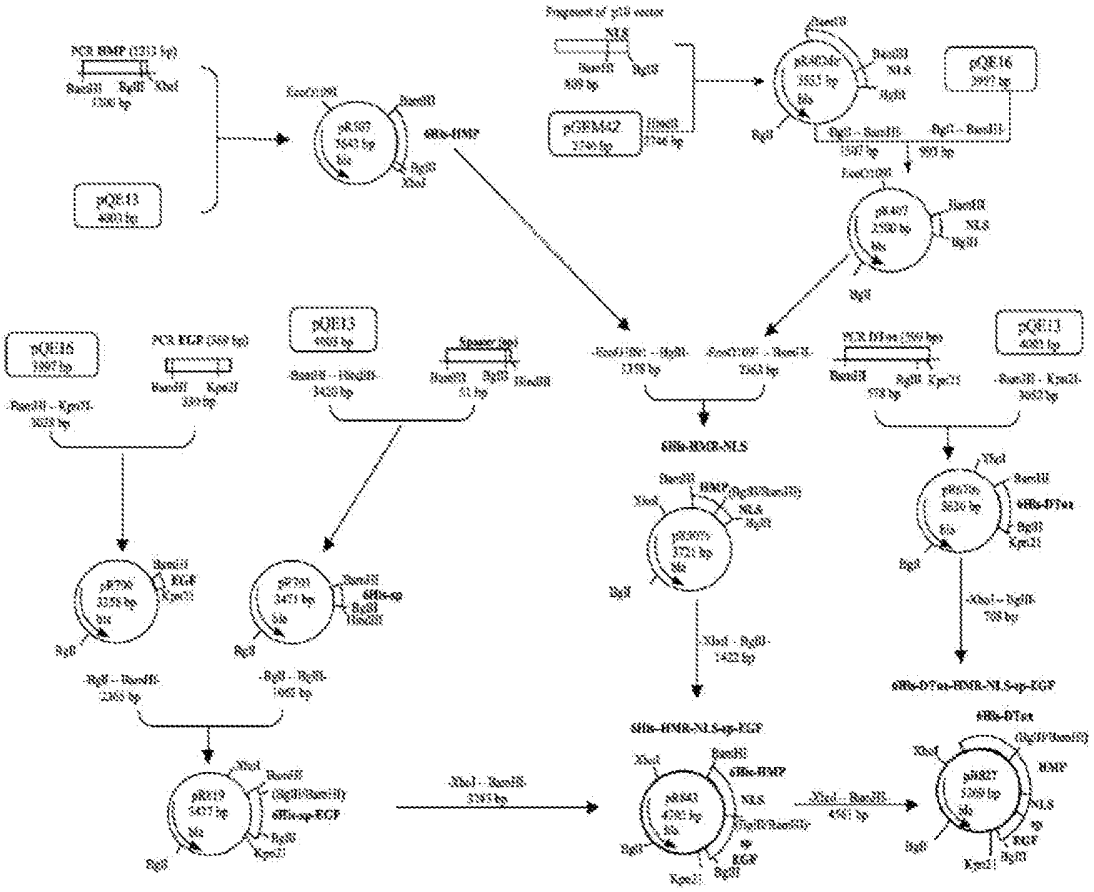


Fig. 6. Schematic representation of plasmid construction to create the plasmid pR827 encoding the EGF-containing MTP DTox-HMP-NLS-EGF.

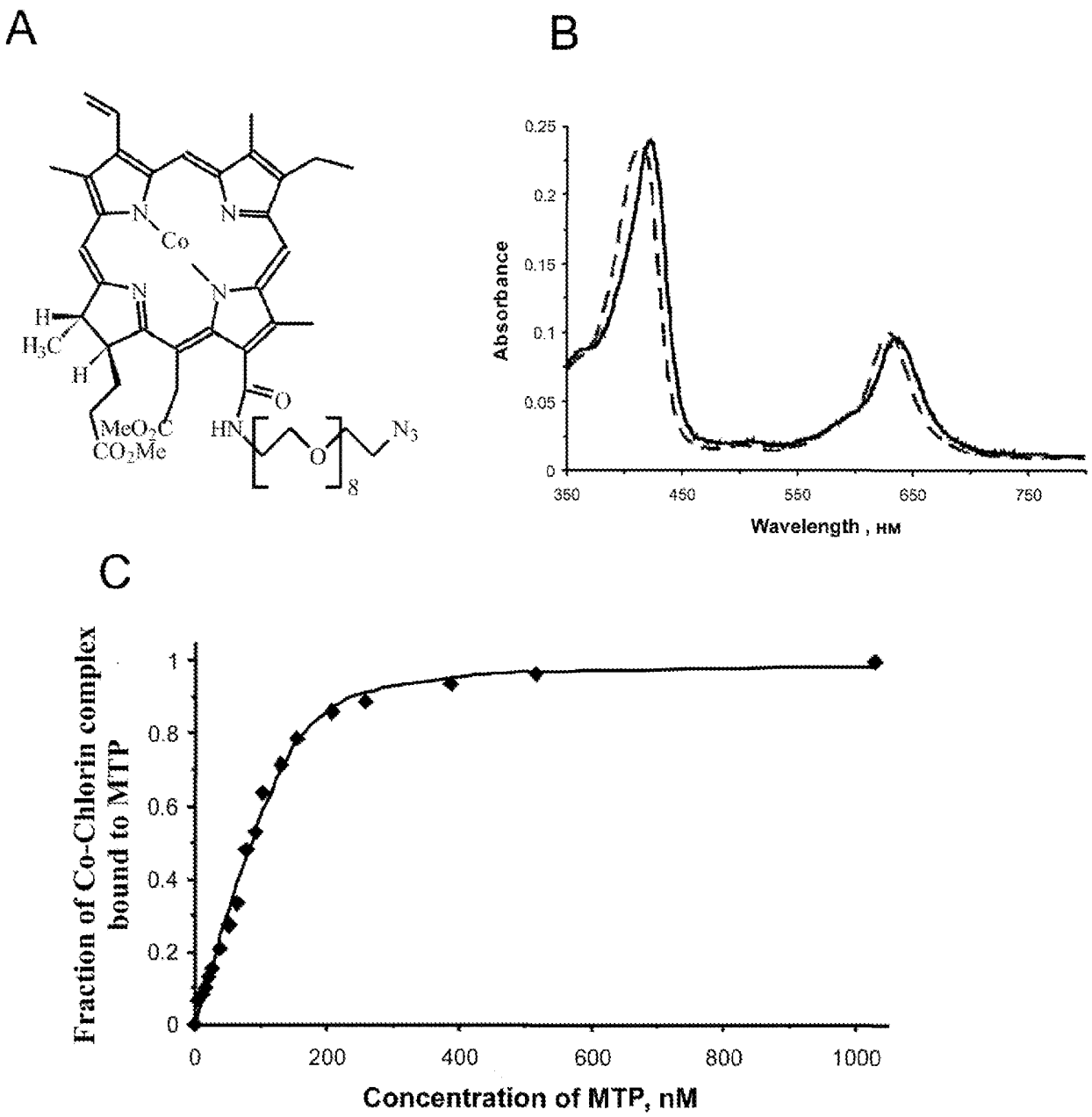


Fig. 7. Insertion of chlorine derivative into MTP. A – azido-polyethylene glycol derivative of Co-chlorin complex (Co-Chl-PEG-N_3); B – absorption spectra of Co-Chl-PEG-N_3 (dashed line) and complex of Co-Chl-PEG-N_3 with DTox-HMP-NLS-MSH MTP (full line) in 10 mM sodium phosphate pH 8.0; C – the dependence of bound Co-Chl-PEG-N_3 share on MRT concentration calculated from MTP-Co-Chl-PEG-N_3 spectra by nonlinear regression from Soret bands of complexes at different MTP concentrations.

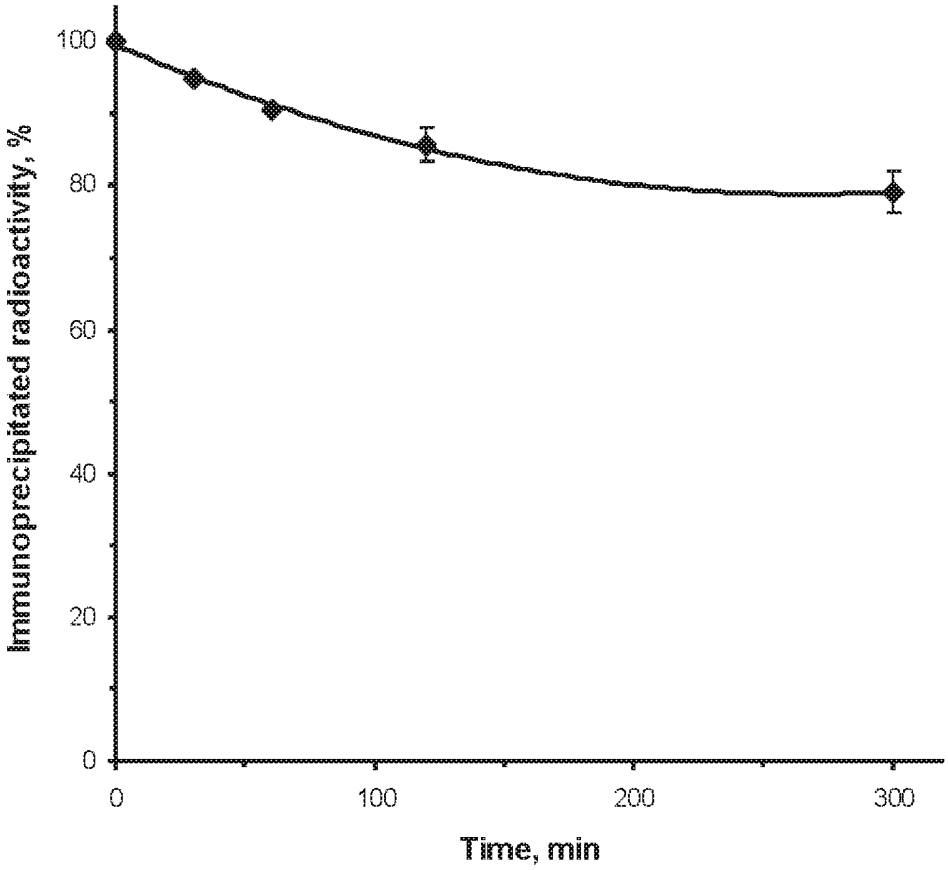


Fig. 8. Immunoprecipitation of ([^{57}Co]-protoporphyrin IX)-MTP complexes after incubation in murine blood plasma for indicated time. The rabbit ant-MNT AB was used for the immunoprecipitation analysis according PICRIA (Shersted H.C., Brandst I., Svehag S.-E., and Jensenius J.C. 1981. Quantitation of circulating immune complexes by combined PEG precipitation and immunoglobin-specific radioimmunoassay (PICRIA). In: Methods in Enzymology, 71: 538-550).

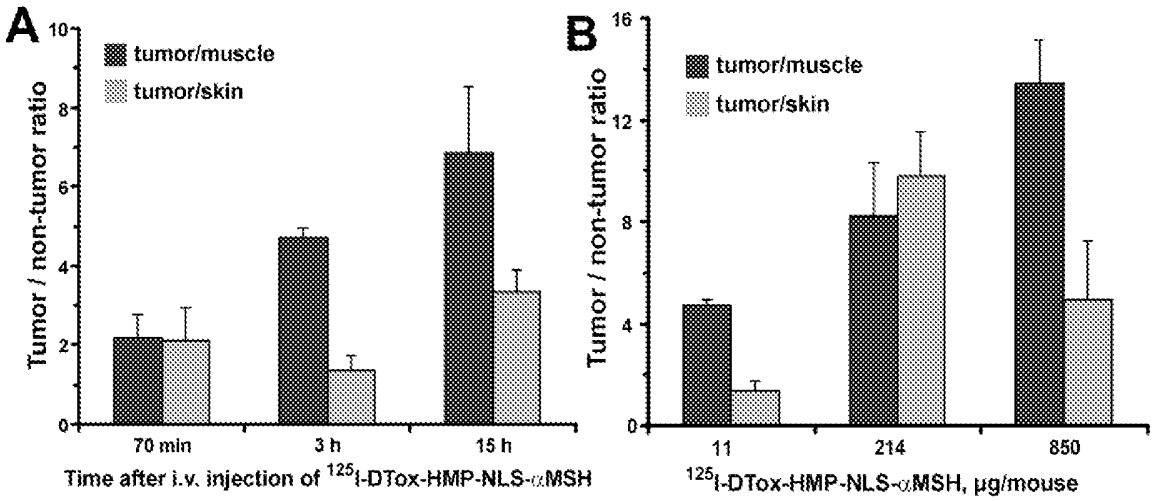


Fig. 9. Tumor-to-tissue ratios of ^{125}I after intravenous injection of ^{125}I-labeled DTox-HMP-NLS- αMSH in B16-F1 melanoma-bearing C57Black/6J mice. (*A*) Effect of time; 11 µg MTP dose. (*B*) Effect of MTP dose; 3 h post injection.

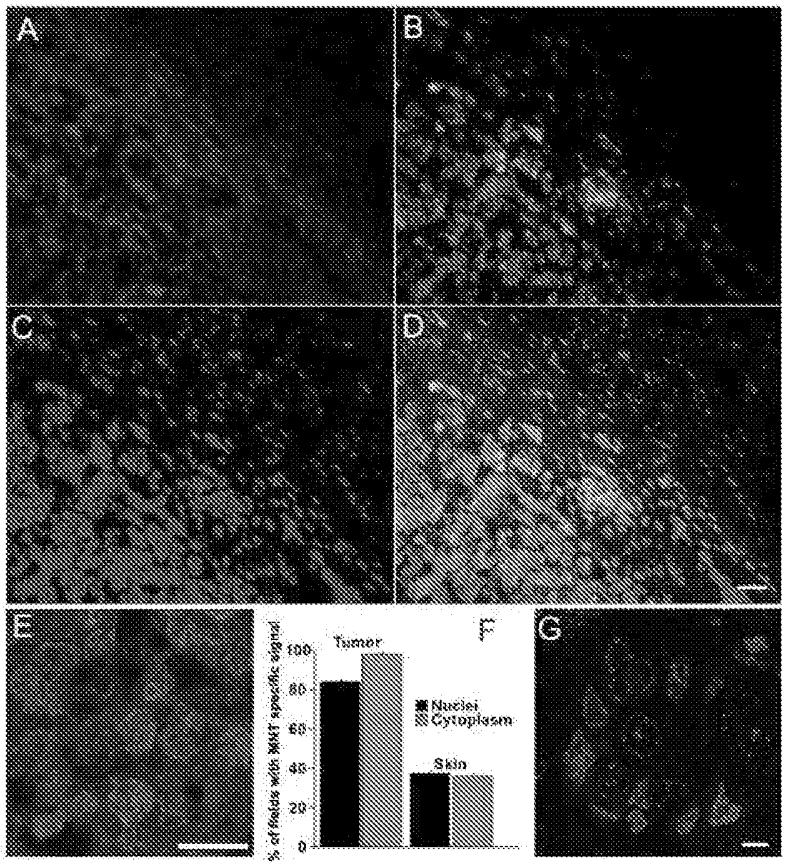


Fig. 10. Immunofluorescence analysis of *in vivo* distribution in tumor and neighboring tissue, and subcellular localization of MTP 3 h after intravenous injection in mice. (*A*)-(*F*) 10 µm tissue sections from DBA/2 mice bearing murine Cloudman melanoma S91 transformed with GFP receiving DTox-HMP-NLS-αMSH. (*A*)-(*D*) tumor and surrounding tissue section (40x). (*A*) Alexa Fluor 555 staining for MTP (red); (*B*) GFP fluorescence from tumor cells (green); (*C*) DAPI staining of cell nuclei (blue); (*D*) overlay of *A*, *B* and *C*. (*E*) tumor section (63x); overlay of DAPI fluorescence (blue) and MTP (red). (*F*) % of fields (± SEM) with specific MTP signal in nuclei and cytoplasm of tumor and neighboring skin cells. (*G*) 2-3 µm tumor section (63x) from Balb/c ByJIco-*nu/nu* mouse bearing human A431 epidermoid carcinoma 3 h after intravenous injection of chlorin e_6-DTox-HMP-NLS-EGF; overlay of DAPI fluorescence (blue) and MTP (red). (Scale bars: *D* and *E*, 20 µm; *G*, 5 µm)

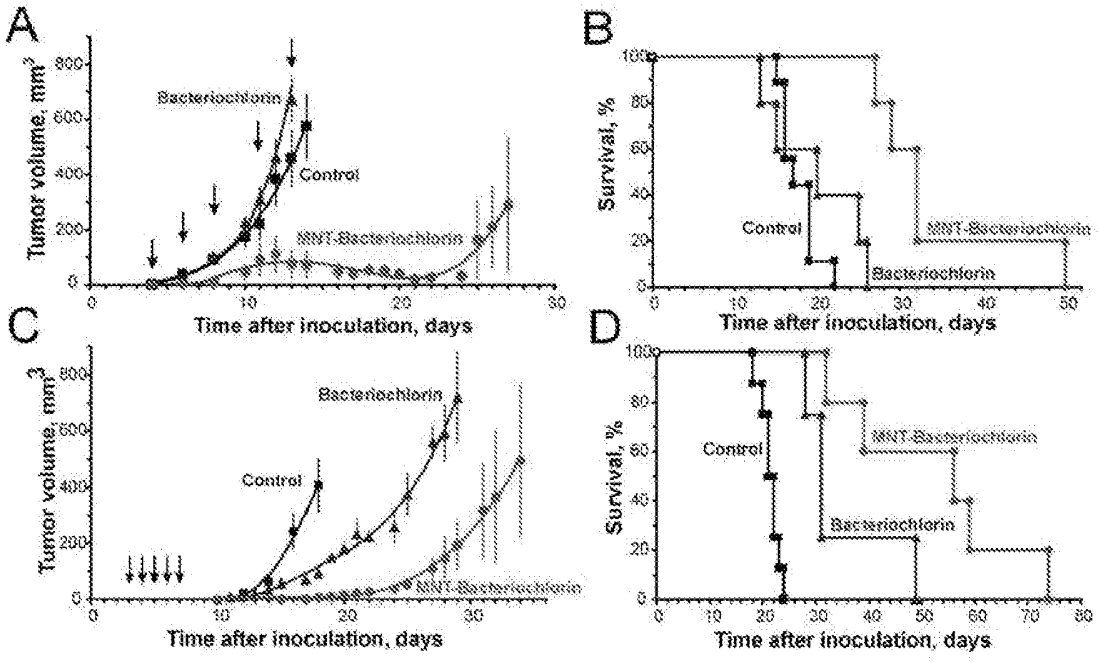


Fig. 11. Comparative efficacy of photodynamic therapy with bacteriochlorin *p* conjugated with DTox-HMP-NLS-αMSH MTP and free bacteriochlorin *p*. (*A*)-(*B*) C57Black/6J mice with subcutaneous B16-F1 murine melanoma; (*A*) tumor growth, mean ± SEM; injection and illumination cycles are indicated with arrows; average tumor volumes are shown up to the last day when all animals were alive in a group. (*B*) Kaplan-Meier survival curves; (*C*)–(*D*) DBA/2 mice with subcutaneous Cloudman S91 murine melanoma; (*C*) tumor growth, mean ± SEM; injection and illumination cycles are indicated with arrows; average tumor volumes are shown up to the last day when all animals were alive in a group. (*D*) Kaplan-Meier survival curves.

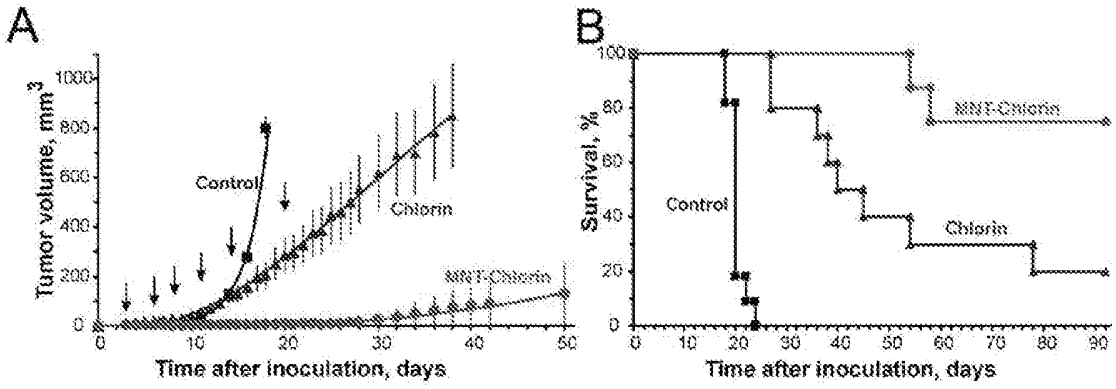


Fig. 12. Photodynamic therapy with chlorin e_6 conjugated with DTox-HMP-NLS-EGF MTP inhibits A431 human epidermoid carcinoma growth and enhances survival of tumor-bearing Balb/c ByJlco-*nu/nu* mice compared with free chlorin e_6. (*A*) A431 tumor growth, mean ± SEM; injection and illumination cycles are indicated with arrows; average tumor volumes are shown up to the last day when all animals were alive in a group. (*B*) Kaplan-Meier survival curves.